ANALYSIS OF A 750 MHZ SRF DIPOLE CAVITY *

A. Castilla[1,2,3†], J. R. Delayen[1,2].

[1]Center for Accelerator Science, Old Dominion University, Norfolk, VA 23529, USA.
[2]Thomas Jefferson National Accelerator Facility, Newport News, VA 23606, USA.
[3]Universidad de Guanajuato (DCI-UG), Departamento de Fisica, Leon, Gto. 37150, Mex.

Abstract

There is a growing interest in using rf transverse deflecting structures for a plethora of applications in the current and future high performance colliders. In this paper, we present the results of a proof of principle (PoP) superconducting rf dipole, designed as a prototype for a 750 MHz crabbing corrector for the Medium Energy Electron-Ion Collider (MEIC), which has been successfully tested at 4.2 K and 2 K at the Jefferson Lab's Vertical Testing Area (VTA). The analysis of its rf performance during cryogenic testing, along with Helium pressure sensitivity, Lorentz detuning, surface resistance, and multipacting processing analysis are presented in this work. Detailed calculations of losses at the port flanges are included for completeness of the cavity's cryogenic performance studies.

INTRODUCTION

Transverse deflectors have been studied for several applications in the past, but when it comes to high performance applications that require compact superconducting designs, a few approaches have been taken. TEM parallel rod cavities showed promising performance for high $\left[\frac{R}{Q}\right]_T$ and after a long evolution and optimization of parameters such as balanced peak surface fields and low multipacting, a TE-like resonant structure was developed by S. U. De Silva *et al* [1,2], known as the rf dipole. The optimization of an rf dipole structure will depend greatly on its applications and machine-specific constraints, from the impedance budget and field flatness to its physical dimensions.

The present work has been prepared as a summary of the efforts devoted to the design and study of a superconducting 750 MHz rf dipole, developed as a PoP crab cavity for the MEIC [3]. A list of its principal parameters and rf properties can be seen in Table 1, while Fig. 1 represents a visualization of the longitudinal (a) and transverse (b) cross sections of the structure.
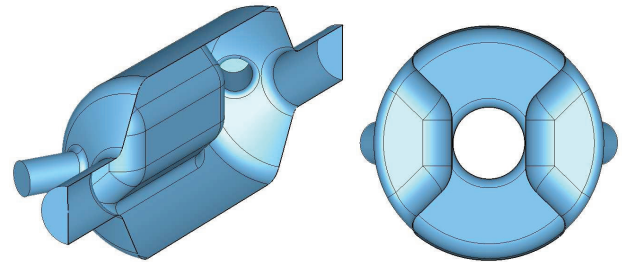
BEAD PULL

The cavity was deep drawn using high grade, large grain, 3mm thick Nb sheets, and e-beam welded. A bulk BCP etching after welding was perfomed by the vendor previous to several preliminary 4.2 K cryogenic tests. Once received at ODU, a series of bead pull measurements were performed to determine the symmetry of the fields (see Figs. 1(a) to

Table 1: RF Dipole Design Parameters

Parameter	750 MHz	Units
$\lambda/2$ of π mode	200.0	mm
Cavity length	341.2	mm
Cavity radius	93.7	mm
Bars width	63.0	mm
Bars length	200.0	mm
Bars angle	45	deg
Aperture diameter -d	60.0	mm
Deflecting voltage -V_T^*	0.20	MV
Peak electric field -E_P^*	4.45	MV/m
Peak magnetic field -B_P^*	9.31	mT
B_P^*/E_P^*	2.09	$\frac{mT}{MV/m}$
Energy content -U^*	0.068	J
Geometrical factor	131.4	Ω
$[R/Q]_T$	124.2	Ω
$R_T R_S$	1.65	$\times 10^4 \Omega^2$

At E_T^*= 1 MV/m

(a) Longitudinal cross section   (b) Transverse cross section

Figure 1: Geometry of the optimized PoP 750 MHz rf dipole.

(c)). Finding the frequency shift due to the perturbation on the fields by a small dielectric (teflon) bead pulled along the cavity's longitudinal axis, the transverse electric field can be determined using Eqn. 1.

$$\left[\frac{\Delta f}{f}\right]_D = -\frac{\pi a^3}{U}\left[\left(\frac{\epsilon_r - 1}{\epsilon_r + 2}\right)\epsilon_0|E|^2\right]. \tag{1}$$

While for a perfect conductor bead, the frequency shift is given by Eqn. 2

$$\left[\frac{\Delta f}{f}\right]_C = -\frac{\pi a^3}{U}\left[\epsilon_0|E|^2 - \frac{\mu_0}{2}|H|^2\right]. \tag{2}$$
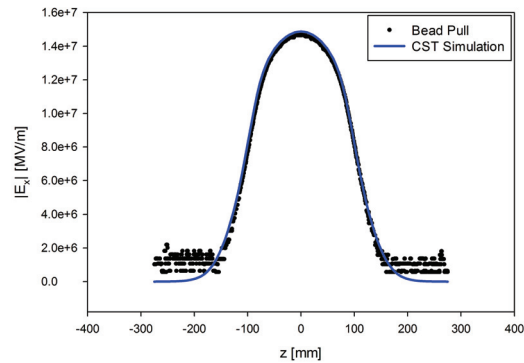
Thus, from Eqns. 1 & 2 we can derive the absolute value for the fields as:

$$|E_x| = \sqrt{\left(\frac{-U}{\pi a^3}\right)\left(\frac{\epsilon_r + 2}{\epsilon_r - 1}\right)\frac{1}{\epsilon_0}\left[\frac{\Delta f}{f}\right]_D},$$
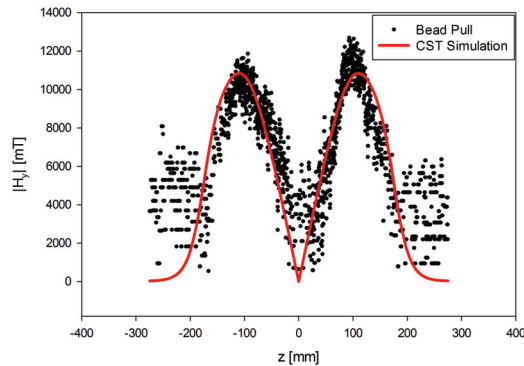
$$|H_y| = \sqrt{\left(\frac{2U}{\pi \mu_0 a^3}\right)\left\{\left[\frac{\Delta f}{f}\right]_C - \left(\frac{\epsilon_r + 2}{\epsilon_r - 1}\right)\left[\frac{\Delta f}{f}\right]_D\right\}}.$$
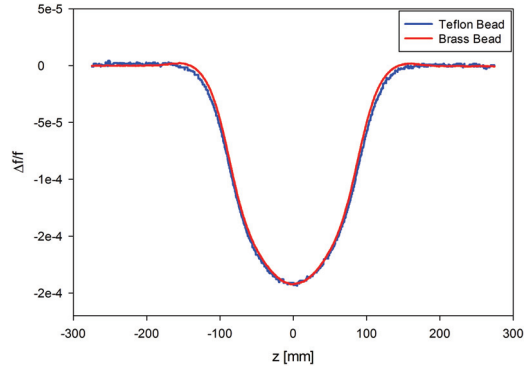
(a) Frequency shift

(b) Transverse electric field

(c) Transverse magnetic field

Figure 2: Bead pull measurements and transverse fields extracted from the numerical simulations.

Figure 2(a) shows the relation of the frequency shifts for both the teflon and the brass beads, while Figures 2(b) and (c) compare respectively the extracted electric and magnetic fields from the bead pull, to the ones obtained by the CST Microwave Studio® simulations (at $U = 1$ J by convention). It is important to say that no scale factors have been used to match the simulated fields to the measurements, other point to highlight is that the system employed is precise enough to allow us to extract the transverse magnetic field profile fairly well, despite the small signal-to-noise ratio. The apparent slight asymmetry of the magnetic field is attributed to errors of alignment between the frequency shift curves (shown in Fig. 2(a)) at the moment of their substraction to calculate the field.

SURFACE TREATMENT

Having performed a bulk BCP on the cavity previously, and for purposes of studying the limitations and flexibility of the rf dipole structure, a 30 μm horizontal electropolishing (HEP) was performed. Due to the complexity of its geometry, the rf dipole presents some challenges for electropolishing surface etching. To address this, the employed aluminum cathode was covered with a dense teflon grid to mask its surface when the distance between this and the cavity surface (anode) was shortest, and correspondingly, making the grid less dense to expose more cathode surface as the distance to the walls was increasing, to procure an uniform etching rate. Figure 3(b) shows in black empty diamonds the measured removal at different locations after the HEP, the highest achieved removals correlate to the points where the distance between the cathode and the walls are shortest (i.e. points 1 and 12 in Fig. 3(a)), while the lowest removals correspond to the points placed in the farthest walls (i.e. 2 to 11 as Fig. 3(a) indicates).

A flash 5 μm buffered chemical polishing (BCP) followed the HEP, with a more uniform thickness removal along the different measured points (shown in Fig. 3(b) as empty red diamonds). This proves that the rf dipole geometry favors the use of BCP, nevertheless, it perfectly allows the use of HEP with a bit of cathode customization, which would be useful when in the search of higher gradients. Figure 3(b) shows in solid blue diamonds, the effective Nb removal at the different measured points after both processes. A thorough high pressure rinse (HPR) was performed after the thickness measurements previous to the final clean assembly.

COOL DOWN MEASUREMENTS

Surface Resistance

Starting from the definition of the surface resistance from the BCS theory:

$$R_S = \left(\frac{A}{T}\right)f^2 e^{-\Delta/k_B T} + R_{\text{res}}, \qquad (3)$$

where A is a material dependant constant, k_B is the Boltzmann constant, f the rf frequency, 2Δ the Nb energy gap, T is the surface temperature, and R_{res} the residual resistance [4].

The methodology followed to determine the residual resistance was to record the Q_0 of the cavity and the temperature of the He bath while cooling down from 4 K to 2 K, at a
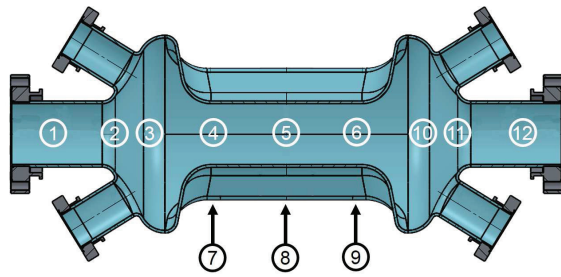
(a) Thickness measurement points
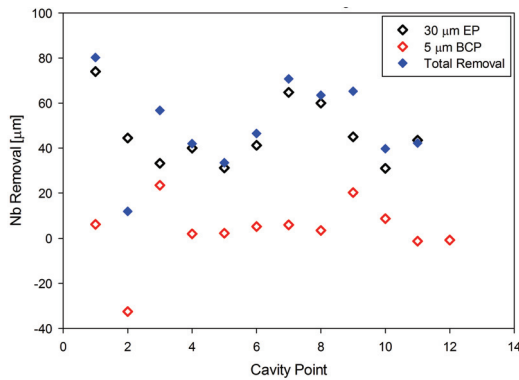
(b) Thickness removal per location

Figure 3: Nb removal after a 30 μm HEP (empty black) and a flash 5μm BCP (empty red).

controled gradient range of $E_T = 0.49$ to 1.99 MV/m. Then, using from Table 1, $G = 131.4\,\Omega$ and the relation:

$$R_S = \frac{G}{Q_0}, \qquad (4)$$

the recorded R_S was plotted against the inverse of the cavity's temperature and fitted using Eqn. 3, leaving A, Δ, and R_{res} as free parameters, with $k_B = 1.38 \times 10^{-4} n\Omega \cdot K \cdot s^2$ and $f = 750$ MHz, obtaining $R_s = 39.34\,n\Omega$ as shown in Fig. 4.
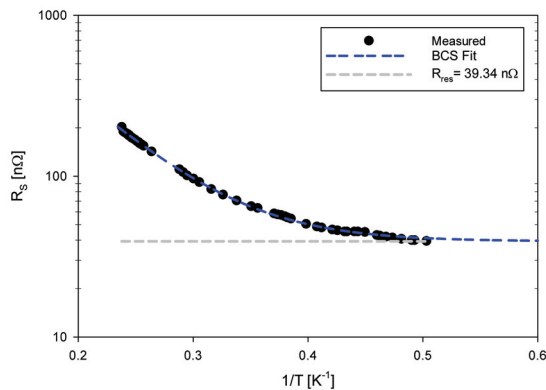

Figure 4: Surface resistance cryogenic measurements.

The residual resistance was found to be almost double as the expected $20\,n\Omega$, even when this could be due to some surface contamination, we have reasons to believe it is consistent with power losses at the S.S. flanges, similar observations have been confirmed previously with other rf dipole designs [5] and the proper calculations and discussion are presented in the *Analysis on Losses* section bellow. The cavity was not baked after etching, low temperature baking could be expected to lower the Q_0, but presumably move the quench point farther up in field level [6].

Helium Pressure Sensitivity

Another important aspect of the structure design is its relative robustness to maintain the resonant frequency within a small range while under stresses exerted by the pressure differences between the ultrahigh vacuum inside the cavity and the He bath it is submersed into. This difference is about 11 orders of magnitude (from an inside vacuum of $\sim 10^{-9}$ to a liquid Helium (LHe) bath of 755 torr).

Plotting the frequency shift as a function of the LHe bath pressure during the cool down, the He pressure sensitivity can be obtained by extracting the slope from a linear fit, which, in the case of the PoP (naked) 750 MHz rf dipole studied in this paper, was found to be $\partial f / \partial P = 0.7$ kHz/torr as shown in Fig. 5. The pressure sensitivity can be easily reduced by adding properly placed stiffening elements to the cavity walls. In order to do so, structural studies using numerical tools can be performed to optimize the place and number of stiffening required, such analysis won't be discussed further in this paper.
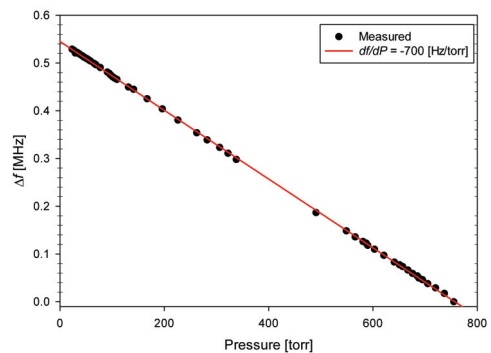

Figure 5: He pressure sensitivity measurements.

CRYOGENIC RF TEST

The Q_0, field levels, and resonant frequency were monitored using the in-house phase locked loop (PLL) system and after placing the cavity under vacuum on the LHe bath at the VTA in Jefferson Lab, both for 4 K and 2 K cases. Using this information we can analyze and study the cryogenic performance of the rf dipole, including: multipacting processing, quenches, field emission, Lorentz detuning, and power losses among other things.

Quality Factor

Figure 6 shows the measured Q_0 at 4 K (black) and at 2 K (blue), as a function of the transverse electric field E_T, the

transverse voltage V_T, and the electric and magnetic peak surface fields E_P and B_P respectively. The empty triangles show the radiation levels measured by the x-ray monitors placed outside the dewar.
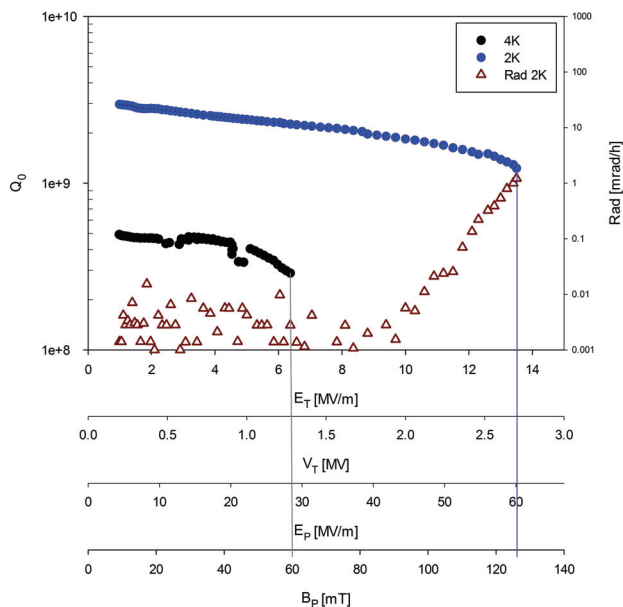

Figure 6: Quality factor at 4 K (black) and 2 K (blue), with radiation measurements (maroon).

The notorious dips on the 4 K (black) Q_0 curve show Q degradation due to multipacting activity, this will be discussed in more detail in the corresponding *Multipacting* section bellow. When it comes to the 2 K (blue) Q_0 curve, there is no strong low field Q slope, however, an evident medium field Q slope can be noticed, as described in Padamsee, *et al* [6], this can be attributed to a non-linear surface resistance, which is a function of the magnetic field, due to grain boundaries, defects, and impurities. A thorough study on this slope may include fairly complex calculations and detailed analysis of the surface composition.

A high field Q slope appears at about E_T = 12 MV/m at 2 K, the ramp up on the x ray emission after E_T = 10 MV/m may indicate activation of field emitters, which could be addressed by He processing. It is worth pointing out that a low temperature baking may push the quenching point further up in gradient. However, it is important to notice the fairly high peak surface fields reached of about E_p = 60 MV/m and B_p = 125 mT, reached at the V_T = 2.7 MV of deflecting voltage at 2 K with a very low x-ray emission ~ 1 mrad/h.

Lorentz Force Detuning

Cavity deformations due to the force exerted on the walls by the radiation pressure can cause a shifting of the resonant frequency, such a force is directed outwards for the case of the magnetic field component and directed inwards for the electric field contribution. This frequency shift is known as Lorentz detuning, for the case of the 750 MHz

rf dipole, the Lorentz coefficient k_L was determined by a linear fit to the recorded frequency shift as a function of the squared of the transverse gradient E_T^2, as can be seen in Fig. 7. The Lorentz coefficient was found to be k_L = −223.4 Hz/$(MV/m)^2$. The high sensitivity to the radiation pressure is due to the relatively large flat surfaces on the loading elements subjected to the high electric fields. The Lorentz coefficient can be improved by adding stiffeners in the areas of higher deformation, and simmilarly to the case of the He pressure sensitivity, in order to reduce this coefficient, numerical studies are necessary to determine the mechanical properties of the structure. In the case of a PoP cavity, such as the one described in the present work, these studies are not relevant, nevertheless and depending on the applications for operating cavities, He pressure sensitivity, Lorentz detuning, as well as promptness to ponderomotive effects can be of high relevance to the specifics of operation and control [7].
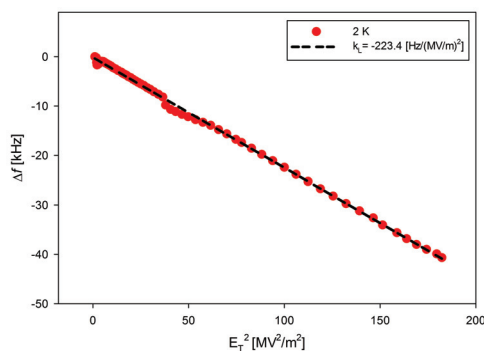

Figure 7: Lorentz detuning measurements.

Multipacting

As mentioned in the *Quality factor* section above, and looking closer to the Q_0 curve obtained at 4 K (shown in solid black in Fig. 8), it is possible to see two clear multipacting barriers occurring at slightly above V_T = 0.4 MV and slightly bellow V_T = 0.9 MV, these barriers have widths in between 0.1 and 0.2 MV and were encountered to be easily broken with an increase of power, their observation was recurrent with following measurements at 4 K. The degree of Q degradation shown depends on the amount of energy put into the multipacting process by the rf fields. Benchmarking the multipacting simulations obtained using TRACK3P from the ACE3P suite, we observed a great consistency between the expected range of voltages for multipacting occurrence and the barriers encountered. The areas affected by multipacting at these levels are mostly the end caps and the high magnetic surface field area on the outer conductor (cavity's top and bottom, so to speak). At 2 K the two barriers were observed in the same voltage levels as expected, but after the first gradient sweep they were successfully cleaned up and they were not observed again. Higher voltage barriers were neither predicted by the simulations nor observed during the test (see the 2 K Q_0 curve (blue) in Fig. 6).
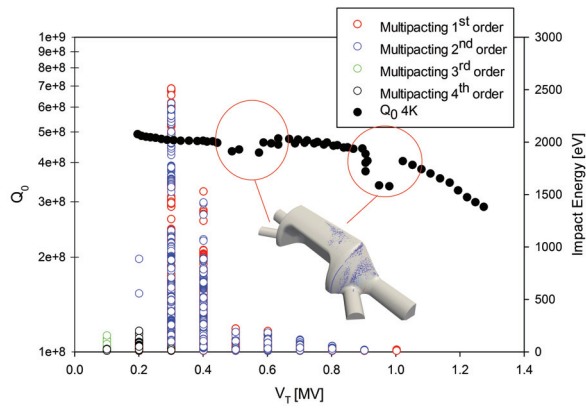
Figure 8: TRACK3P simulation (empty dots) and multipacting barriers encountered during the test (solid dots).

ANALYSIS ON LOSSES

In this section, we calculate the power dissipated on the flanges due to Ohmic losses generated by the residual magnetic field at their location. In order to do this, we will consider the total loss as the sum over the 2 beam pipes and the 4 auxiliar ports' flanges. The time-averaged power dissipated at the flanges per unit area due to the rf fields can be expressed as:

$$\frac{dP_{\text{loss}}}{dA} = \frac{R_S}{2}|\mathbf{H}_{||}|^2, \tag{5}$$

then, the dissipated power by one of the flanges is:

$$P_{\text{loss}} = \frac{R_S}{2}\iint |\mathbf{H}_{||}|^2 dA. \tag{6}$$

For the rf dipole's fundamental mode, $\mathbf{H}_{||}$ corresponds to $\mathbf{H}_y$, while the integral is bounded to the area of the flanges exposed to the fields. R_S is the resistance presented to the rf fields by the flanges' surface and can be expressed in terms of the material's conductivity σ_m and the rf frequency ω as shown in Eqn. 7.

$$R_S = \sqrt{\frac{\mu_0\omega}{2\sigma_m}}, \tag{7}$$

where m refers to Copper or Stainless Steel.

The 3D fields were extracted from the CST Microwave Studio® simulations, a script to calculate the numerical area integral of the field at the flanges location was written. Quality factors associated to the total power dissipated by all the flanges ΣP_{loss} can be calculated using Eqn. 8, and the results are presented in Table 2.

$$Q_0 = \frac{\omega U}{\Sigma P_{\text{loss}}}. \tag{8}$$

Table 2: Power Dissipated by the Flanges at $U = 1$ J

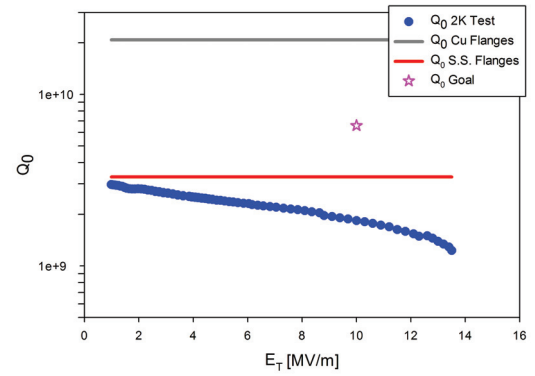| Material	σ_m [S/m]	ΣP_{loss} [W]	Q_0
Copper	5.80×10^7	0.2265	2.08×10^{10}
Stainless Steel	1.45×10^6	1.4324	3.29×10^9

Figure 9: Measured Q_0 for the cavity (blue), Q_0 associated to the losses on the flanges for Cu (grey) and S.S. (red).

The goal Q_0 shown in Fig. 9 (star) was calculated using Eqn. 4, for $R_{\text{res}} = 20\,n\Omega$ and $R_{BCS} = 4\,n\Omega$ at 2 K. The measured Q_0 at 2 K is very close to the expected value when the power dissipation is dominated by the losses at the S.S. flanges.

CONCLUSIONS

Bead pull measurements were presented in agreement with the numerical simulations. The surface resistance analysis showed to be consistent with losses on the S.S. flanges, suggesting the use of Cu flanges to reach a better Q_0 at 2 K. The He pressure sensitivity and the Lorentz detuning of the bare PoP cavity were found to be $df/dP = 0.7$ kHz/torr and $K_L = 223.4$ Hz/$(MV/m)^2$ respectively. Soft multipacting barriers were observed at the expected gradient regions according to the simulations, but were easily processed and did not compromised the cavity's performance. The field levels achieved in the 2 K test were considerably high: $E_T = 13.50$ MV/m, peak surface fields of $E_p = 60.08$ MV/m and $B_p = 125.69$ mT, which are fairly close to the practical limits, all of these for a transverse voltage of $V_T = 2.70$ MV before quenching.

REFERENCES

[1] S.U. De Silva and J.R. Delayen, Phys. Rev. ST Accel. Beams 16, 012001 (2013).

[2] S.U. De Silva and J.R. Delayen, Phys. Rev. ST Accel. Beams 16, 082001 (2013).

[3] S. Abeyratne, et al, "Science Requirements and Conceptual Design for a Polarized Medium Energy Electron-Ion Collider at Jefferson Lab", JLAB-ACC-12-1619 (2012).

[4] J. Bardeen et al., "Theory of Superconductivity", Phys. Rev. Vol. 108 No. 5, p. 1175 (1957).

[5] S.U. De Silva, Ph. D. Thesis, Old Dominion University, Norfolk, VA (2014).

[6] H. Padamsee, "RF Superconductivity", ISBN 978-3-527-40572-5, WILEY-VCH, Germany (2009).

[7] J. R. Delayen, in Proceedings of SRF 2005, Ithaca, New York, p. 35 (2005).